Sensor-less Speed and Flux Control of Dual Stator Winding Induction Motors Based on Super Twisting Sliding Mode Control

Mojtaba Ayaz Khoshhava, Hossein Abootorabi Zarchi, and Gholamreza Arab Markadeh

***Abstract*—This paper proposes a direct speed and flux control system for Dual Stator Winding Induction Machines (DSWIMs) based on Super Twisting Sliding Mode Control (STSMC). The proposed nonlinear controller which has finite time convergence of error to zero, is designed such that the Lyapunov stability condition is satisfied. Furthermore, a novel torque-sharing algorithm is introduced for DSWIMs. This algorithm enables them to operate in a wide speed region, including zero speed, such that the required electromagnetic torque is supplied by two winding sets based on their power ratings. In addition, a Sliding Mode Control (SMC) based full order observer is proposed for DSWIMs. This observer, which is able to estimate the winding fluxes, flux angles and rotor speed with high-accuracy, guarantees the optimal flux condition. The functionality of the proposed sensor-less DSWIM drive scheme is evaluated through some experimental tests performed on a 3.3 kW DSP-based DSWIM drive system. The experimental results confirm the effectiveness of the proposed control method, torque sharing algorithm and the full order observer in various speed regions.**

***Index Terms*—Dual stator winding induction machines (DSWIMs), super twisting sliding mode controller (STSMC), sliding mode full order observer, torque sharing algorithm.**

NOMENCLATURE

V,I and λ	Voltage, Current and Flux
Φ_{DC}	DC machine flux
p_i	Number of poles of the ith winding set
θ_i	The flux angle of each winding set respect to the *A* winding axis of the *ABC* winding set
ω_s *and* ω_r	Synchronous speed and Rotor speed
B_{gi}	The amplitude of the flux density of the ith winding set
B_{gt}	Total air-gap flux density
δ	The relative angle between the flux densities of the stator winding sets
R_{si}	Stator resistance of the ith winding
R_{ri}	Rotor resistance respect to the ith winding
L_{ri}	Rotor self-inductance respect to the ith winding
L_{mi}	Magnetizing inductance of the ith winding
L_{si}	Stator self-inductance of the ith winding
J	Moment of inertia
T_{ei}, T_L *and* T_R	Electromagnetic torque produced by the ith winding set, the total load and the resistive load torques

Subscripts

s and r	Stator and rotor
$i = 1$ *and* 2	*ABC and XYZ*

Superscripts

hate	Estimated parameters
prime	Rotor parameters referred to stator
star	Reference parameters

Manuscript received October 16, 2020; revised February 19, 2021; accepted May 1, 2021. Date of publication May 5, 2021; date of current version November 23, 2021. Paper no. TEC-01036-2020. *(Corresponding author: Hossein AbootorabiZarchi.)*

Mojtaba Ayaz Khoshhava and Hossein Abootorabi Zarchi are with the Department of Engineering, Ferdowsi University of Mashhad, 9177948944 (e-mail: mojtaba.ayaz@mail.um.ac.ir; abootorabi@um.ac.ir).

Gholamreza Arab Markadeh is with the Department of Engineering, Shahrekord University, 8818634141 (e-mail: arab-gh@eng.sku.ac.ir).

Color versions of one or more figures in this article are available at https://doi.org/10.1109/TEC.2021.3077829.

Digital Object Identifier 10.1109/TEC.2021.3077829

I. INTRODUCTION

THE interest in dual winding induction machines due to their superiorities over single winding machines, has significantly increased in recent years. These advantages can be addressed as higher redundancy, broader range of operation and higher power rating. According to their rotor structure, these machines are categorized into two principal groups: *nested loop* and *squirrel cage* [1]. The nested loop rotor structure involves high fabrication costs and it is adapted in Brushless Doubly Fed Induction Machines (BDIFMs) which have two sets of three phase windings with different pole pairs in their stator [2]. Although BDFMs have narrow operation speed region, they have been adapted for various motoring and generating applications [3]. The second group can be further branded into two categories which are similar pole pairs (split-wound) and dissimilar pole pairs (Dual Stator Winding Induction Machines (DSWIMs)). The split-wound machines adapt standard squirrel cage rotors and their stator has two sets of similar pole three phases windings. Due to the adaptation of a similar pole pair arrangement for stator winding sets, there exists direct coupling between stator windings of these machines. Thus, small voltage unbalances can result in high circulating currents [4].

DSWIMs have been first introduced in 1998 [5]. The rotor of these sorts of dual winding induction machines is similar to that of split-wound machines; however, their stator winding sets have been wound for unequal pole pairs. This structure results in

completely independent operation of winding sets. Some of the advantages of DSWIMs over other sorts of induction machines can be enumerated as [6]:

- Simpler structure and lower fabrication costs in comparison to BDFIMs.
- In contrast to split wound machines, in case of voltage unbalance, there is no circulating current between the two winding sets.
- Wider operating speed region compared to BDFIMs.
- Improved control in flux weakening region in comparison to Single Winding Induction Machines (SWIMs).
- The capability of working in zero and very low speed operation regions deprived of the controllability difficulties exists in SWIMs. This advantage makes DSWIMs excellent candidate for sensor-less applications.

According to the above-mentioned advantages, DSWIM can be adapted for various motoring and generating applications. As the operation of winding sets are completely independent of each other, they can be adapted as generators to generate different voltage levels [23]–[24]. As DSWIMs has virtuous performance in a wide speed region including very low and zero speed region, they can be appropriate candidates for adapting in motoring applications, which require high controllability in this operation region such as elevators and electrical vehicles.

Already the scalar and Indirect Field Oriented Control (IFOC) methods has been proposed for DSWIMs [7]–[13]. The other family of control strategies for induction machines is the Direct Torque and flux control (DTC). DTC is free of current control loops and has faster dynamic response in comparison to other control strategies. Moreover, it is easy to implement in various IM drive system, especially sensor-less schemes. Despite these advantages, classic DTC involves some drawbacks as large torque, flux, and current ripple, producing acoustical noise, including nonzero steady-state torque error, complications in controlling the flux at low speeds, and variable switching frequency [15]. One of the most promising methods to overcome these disadvantages is the implementation of Variable Structure Control (VSC) methods [25]. The VSC is an effective control method for nonlinear systems with uncertainties. The advantages of VSC can be enumerated as being a high- frequency switching control strategy, robustness against parameter variations and other disturbances and fast dynamic response. One of the most promising VSC schemes is the Sliding Mode Controller (SMC). The advantages of SMC are the simple implementation, disturbance rejection, robustness, having fixed switching frequency and fast dynamic response [15]. Nevertheless, it involves chattering and its stabilization time may be infinite. To overcome these drawbacks, the PI-SMC has been proposed in [14] in a DTC DSWIM drive system. However, in this method a discrete control action is necessary, which needs to apply high switching frequency to the inverter. In addition, the implementation of PI controller decreases the speed of dynamic response.

In this paper, the Super Twisting Sliding Mode Controller (STSMC) is proposed for direct speed and flux control of DSWIMs. STSMC is an advanced theory in the SMC design and its effectiveness has been proven for electromagnetic systems [26]. Unlike other Second Order Sliding Mode (SOSM) controllers, STSMC is applicable to a system (in general with any order) where the control appears in the first derivative of the sliding variable [27]. The most significant advantage of STSMC is that it is free of the time derivative of the sliding surface (dS/dt). STSMC does not have a discrete output and mitigates the chattering, while the advantages of SMC in the static and dynamic performance are preserved. Other advantages of STSMC are robustness against various internal and external disturbances and model uncertainties, having finite-time convergence, relatively simple control laws, lower torque ripple and THD in comparison to PI-SMC and requiring only the information of the output (sliding variables) [27]. In addition, implementing this controller guarantees the Lyapunov stability condition. The key novelties and unique characteristics of the DSWIM drive system proposed in this article are listed as follows:

1) Implementing the STSMC method for DSWIM direct Speed and flux control. The proposed control system guarantees the Lyapunov stability condition. Besides, it has finite time convergence of error to zero.
2) Introducing an innovative torque-sharing algorithm, which prevents windings from overloading in various operating conditions and enables the drive system to appropriately control the rotor speed in the zero speed region.
3) This drive system is free of position and speed sensors. This is achieved through a Sliding Mode Observer (SMO). On contrast to other sensor-less methods proposed for DSWIM to date, this method is free of exact machine parameters information and it is robust against parameters variations.
4) The proposed drive system guarantees for optimal flux condition free of speed or position sensors in the synchronous operation mode and enables the convenient flux estimation in the various operation conditions.

II. DSWIM Modeling

As stated in the previous section, in a DSWIM there is no coupling between the two winding sets. Thus, a DSWIM can be considered as two independent three-phase induction machines coupled via a common shaft. Consequently, the d-q equivalent electrical model of a DSWIM is as Fig. 1 [7].

The air-gap flux in a DSWIM is sum of the air-gap fluxes produced by each of the winding sets. Consider a DSWIM with two pole and six pole windings combination. The total air-gap flux density equals [16]:

$$B_{gt} = B_{g1}\cos(\theta) + B_{g2}\cos(3\theta + \delta) \tag{1}$$

In [11] it is declared that keeping δ at 180^{o} results in optimal iron utilization. If it is supposed that the control system guarantees the optimal condition for δ, the following assumptions are made in the stator flux reference frame:

$$\begin{cases} \lambda_{qs1} = 0 \\ \lambda_{ds1} = \lambda_{s1} \end{cases} \tag{2}$$

$$\begin{cases} \lambda_{qs2} = 0 \\ \lambda_{ds2} = -\lambda_{s2} \end{cases} \tag{3}$$

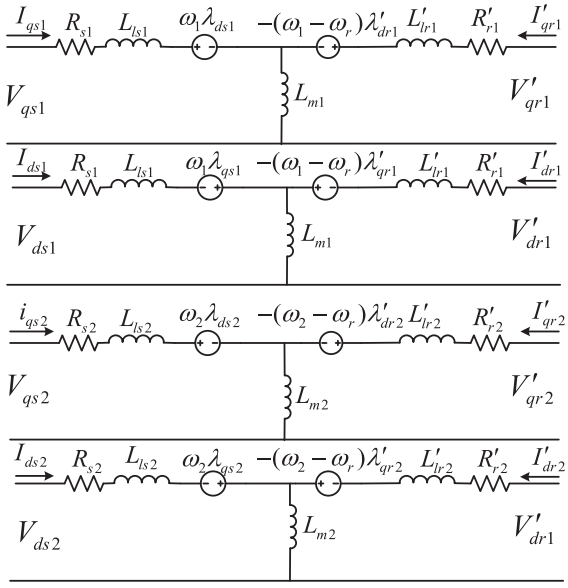

Fig. 1. DSWIM equivalent electrical model.

According to the above assumptions and Fig. 1, the stator and rotor voltage equations for the *ABC* winding set are as follows:

$$V_{ds1} = R_{s1}I_{ds1} + \frac{d\lambda_{s1}}{dt} \tag{4}$$

$$V_{qs1} = R_{s1}I_{qs1} + \omega_1\lambda_{s1} \tag{5}$$

$$V'_{dr1} = R'_{r1}I'_{dr1} + \frac{d\lambda'_{dr_1}}{dt} - (\omega_1 - \omega_r)\lambda'_{qr1} = 0 \tag{6}$$

$$V'_{qr1} = R'_{r1}I'_{qr1} + \frac{d\lambda'_{qr1}}{dt} + (\omega_1 - \omega_r)\lambda'_{dr1} = 0 \tag{7}$$

Where:

$$\lambda_{ds1} = L_{s1}I_{ds1} + L_{m1}I'_{dr1} = \lambda_{s1} \tag{8}$$

$$\lambda_{qs1} = L_{s1}I_{qs1} + L_{m1}I'_{qr1} = 0 \tag{9}$$

$$\lambda'_{dr1} = L_{m1}I_{ds1} + L'_{r1}I'_{dr1} \tag{10}$$

$$\lambda'_{qr1} = L_{m1}I_{qs1} + L'_{r1}I'_{qr1} = \left[L_{m1} - \frac{L'_{r1}L_{s1}}{L_{m1}}\right] I_{qs1} \tag{11}$$

Likewise, the voltage equations for the *XYZ* winding set are as follows:

$$V_{ds2} = R_{s2}I_{ds2} - \frac{d\lambda_{s2}}{dt} \tag{12}$$

$$V_{qs2} = R_{s2}I_{qs2} - \omega_2\lambda_{s2} \tag{13}$$

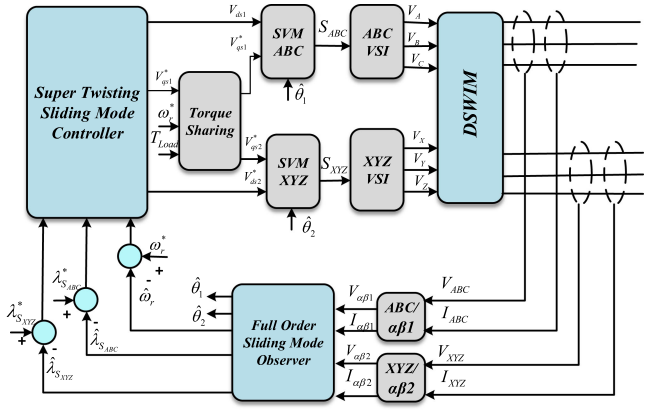

Fig. 2. Proposed DSWIM drive system.

$$V'_{dr2} = R'_{r2}I'_{dr2} + \frac{d\lambda'_{dr2}}{dt} - (\omega_2 - \omega_r)\lambda'_{qr2} = 0 \tag{14}$$

$$V'_{qr2} = R'_{r2}I'_{qr2} + \frac{d\lambda'_{qr2}}{dt} + (\omega_2 - \omega_r)\lambda'_{dr2} = 0 \tag{15}$$

Where:

$$\lambda_{ds2} = L_{s2}I_{ds2} + L_{m2}I'_{dr2} = -\lambda_{s2} \tag{16}$$

$$\lambda_{qs2} = L_{s2}I_{qs2} + L_{m2}I'_{qr2} = 0 \tag{17}$$

$$\lambda'_{dr2} = L_{m2}I_{ds2} + L'_{r2}I'_{dr2} \tag{18}$$

$$\lambda'_{qr2} = L_{m2}I_{qs2} + L'_{r2}I'_{qr2} = \left[L_{m2} - \frac{L'_{r2}L_{s2}}{L_{m2}}\right] I_{qs2} \tag{19}$$

The electromagnetic torque produced by the *ABC* and *XYZ* winding sets are calculated as (20) and (21), respectively.

$$T_{e1} = \frac{3}{4}P_1 I_{qs1}\lambda_{s1} = k_1 I_{qs1}\lambda_{s1} \tag{20}$$

$$T_{e2} = -\frac{3}{4}P_2 I_{qs2}\lambda_{s2} = -k_2 I_{qs2}\lambda_{s2} \tag{21}$$

The electromagnetic torque of a DSWIM is sum of the electromagnetic torques produced by each winding set. Consequently, the mechanical equation is as follows:

$$T_{e1} + T_{e2} - T_L = J\frac{d\omega_r}{dt} + B\omega_r \tag{22}$$

III. Proposed DSWIM Drive System

The proposed DSWIM drive system is depicted in Fig. 2. As illustrated, in this system, the measured voltages and currents are transferred to the $\alpha\beta$ form by the Clark Transformation. Based on the transferred voltages and currents, the SMC based

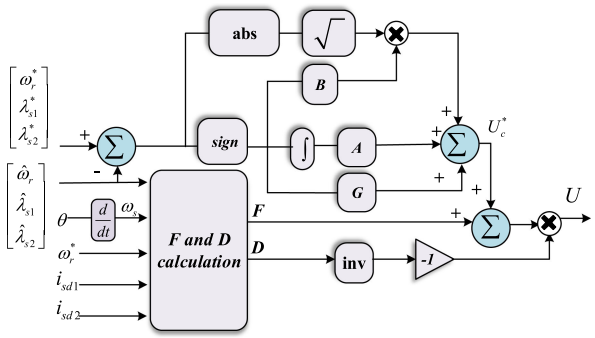

Fig. 3. The block-diagram of the proposed STSMC.

full order observer, estimates the windings fluxes magnitudes, the rotor speed, $\hat{\theta}_1$ and $\hat{\theta}_2$. After that, the STSMC determines the reference values for the d-axis voltages of *ABC* and *XYZ* winding sets and the reference value of the q-axis voltage for the *ABC* winding set based on the errors of the winding fluxes and rotor speed. The proposed torque-sharing algorithm according to the load torque, the reference speed and the determined q-axis reference voltage of the *ABC* winding set, fixes the value of the q-axis voltage for the *XYZ* winding set. Along with the reference d-axis and q-axis voltages, the SVM blocks determine the appropriate switching commands for the Voltage Source Inverters (VSIs), which supply the stator winding sets.

A. Super Twisting Sliding Mode Controller

The proposed STSMC block diagram is shown in Fig. 3. This controller is designed such the Lyapunov stability condition is guaranteed. The sliding surface vector (*S*) is defined as:

$$S = \begin{bmatrix} s_1 \ s_2 \ s_3 \end{bmatrix}^T = \begin{bmatrix} \omega_r^* - \omega_r \ \lambda_{s1}^* - \lambda_{s1} \ \lambda_{s2}^* - \lambda_{s2} \end{bmatrix}^T \quad (23)$$

Consider the Lyapunov function as (24):

$$W = \frac{1}{2} S^T S \quad (24)$$

As *W* is positive definite, if it is proved that $\dot{W} = S^T \frac{dS}{dt} < 0$, the stability of the control system will be guaranteed. Considering the reference stator fluxes change step-wisely, from (23) and (4-22), the derivate of the sliding vector is calculated as:

$$\frac{dS}{dt} = \begin{bmatrix} \dot{\omega}_r^* - \frac{1}{J}(T_{e1} + T_{e2} - B\omega_r - T_L) \\ -(V_{ds1} - R_{s1} I_{ds1}) \\ (V_{ds2} - R_{s2} I_{ds2}) \end{bmatrix} \quad (25)$$

The torque-sharing algorithm determines a linear relation between the electromagnetic torques of winding sets as $T_{e1} = k_T T_{e2}$. Accordingly, from (5) and (20), (25) is rewritten as:

$$\frac{dS}{dt} = \begin{bmatrix} \dot{\omega}_r^* - \frac{1}{J}((1+k_T)k_1\left(\frac{V_{qs1} - \omega_s \lambda_{s1}}{R_{s1}}\right)\lambda_{s1} - B\omega_r - T_L) \\ -(V_{ds1} - R_{s1} I_{ds1}) \\ (V_{ds2} - R_{s2} I_{ds2}) \end{bmatrix} \quad (26)$$

Defining the control input vector as $U = \begin{bmatrix} V_{qs1} \ V_{ds1} \ V_{ds2} \end{bmatrix}^T$, one can rewrite (26) as (27).

$$\frac{dS}{dt} = F + DU + \Delta C \quad (27)$$

Where, *D* and *F* are defined as (28) and (29), respectively. In (27), ΔC is added due to unknown stator resistance, moment of inertia and viscosity. Thus, it is calculated as (30).

$$D = \begin{bmatrix} -\frac{1}{J}((1+k_T)k_1(\frac{\lambda_{s1}}{R_{s1}}) & 0 & 0 \\ 0 & -1 & 0 \\ 0 & 0 & 1 \end{bmatrix} \quad (28)$$

$$F = \begin{bmatrix} \dot{\omega}_r^* - \frac{1}{J}((1+k_T)k_1\left(\frac{-\omega_s \lambda_{s1}^2}{R_{s1}}\right) - B\omega_r - T_L) \\ R_{s1} I_{ds1} \\ -R_{s2} I_{ds2} \end{bmatrix} \quad (29)$$

$$\Delta C = \begin{bmatrix} \Delta B\hat{\omega}_r + \Delta T_{load} + x \\ \Delta R_{s1} I_{ds1} \\ \Delta R_{s2} I_{ds2} \end{bmatrix} \quad (30)$$

In (28-30), nominal parameters are adapted to calculated F, D and ΔC. The Δ sign before each parameter shows the uncertainty in that parameter and *x* equals:

$$x = (1+k_T)k_1\omega_s\lambda_{s1}^2 \times \left(\frac{\Delta J R_{s1} + J\Delta R_{s1} + \Delta J \Delta R_{s1}}{J R_{s1}(J R_{s1} + \Delta J R_{s1} + J\Delta R_{s1} + \Delta J \Delta R_{s1})}\right) \quad (31)$$

If *U* is defined as $U = -D^{-1}[F + U_C^*]$, the Lyapunov stability condition could be satisfied. Since, U_C^* equals:

$$U_C^* = \int A sign(S) + B\,|S|^{1/2} sign(S) + G sign(S) \quad (32)$$

In (30), *sign(S)* stands for the sign function and *A*, *B* and *G* are the control gain matrices and they are defined as:

$$A = \begin{bmatrix} a_{11} \ a_{12} \ a_{13} \\ a_{21} \ a_{22} \ a_{23} \\ a_{31} \ a_{32} \ a_{33} \end{bmatrix}, \ B = \begin{bmatrix} b_1 \ b_2 \ b_3 \end{bmatrix}^T, \ G = \begin{bmatrix} g_1 \ g_2 \ g_3 \end{bmatrix}^T$$

According to (27), (32) and the definition of *U*, (27) is rewritten as:

$$\frac{dS}{dt} = -\left[\int A sign(S) + B\,|S|^{1/2} sign(S) + G sign(S)\right] + \Delta C \quad (33)$$

Thus, the derivate of the proposed Lyapunov function will be:

$$\dot{W} = S^T \frac{dS}{dt} = -S^T\left[\int A sign(S) + B\,|S|^{1/2} sign(S) + G sign(S)\right] + S^T \Delta C \quad (34)$$

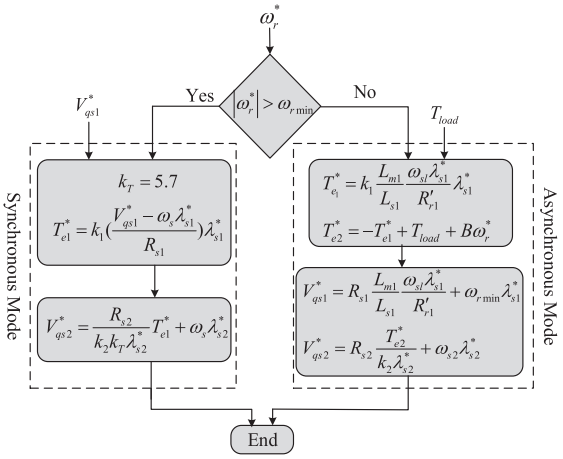

Fig. 4. The proposed torque sharing algorithm flowchart.

As a result, by selecting any positive value for a_{ij} and b_i, the first two terms are negative definite. If $G|S| > S^T \Delta C$, the Lyapunov stability is confirmed for the control system. Thus, G is selected as:

$$G = \begin{bmatrix} g_1 \\ g_2 \\ g_3 \end{bmatrix} = \begin{bmatrix} \Delta B_{\max}\omega_{r\max} + \Delta T_{L\max} + x_{\max} \\ \Delta R_{s1\max} I_{ds1\max} \\ \Delta R_{s2\max} I_{ds2\max} \end{bmatrix} \quad (35)$$

Where, the subscribe *max* stands for the maximum value of each parameter.

B. Torque Sharing Algorithm

The torque sharing algorithm flowchart is illustrated in Fig. 4. As it is shown, there are two modes of operation for DSWIMs: the synchronous and the asynchronous modes.

a) Synchronous mode: in the synchronous operation mode, both winding sets cooperate to supply the load torque and the supply frequency of them has a ratio equal to their pole pair ratio. Thus, their synchronous speed is equal to each other. In this mode, the reference speed is above a minimum value (ω_{rmin}) and the torque is shared between winding sets based on their nominal power. This way, no over-loading occurs for winding sets. Substituting I_{qs1} from (4) into (20), the reference electromagnetic torque for *ABC* winding set is calculated as:

$$T_{e1}^* = k_1 \left(\frac{V_{qs1}^* - \omega_s\lambda_{s1}^*}{R_{s1}} \right) \lambda_{s1}^* \quad (36)$$

Considering a linear relation between the electromagnetic torques of winding sets as $T_{e1} = k_T T_{e2}$, the reference value for the q-axis voltage of the *XYZ* winding set equals:

$$V_{qs2}^* = \frac{R_{s2}}{k_2 k_T \lambda_{s2}^*} T_{e1}^* + \omega_s\lambda_{s2}^* \quad (37)$$

As the DSWIM under study has the stator winding sets with 2850W and 500W rated powers, the torque-sharing factor (k_T) is 5.7.

b) Asynchronous mode: in this mode of operation the frequency of the *ABC* winding set is clamped to a minimum value ($\omega_{rmin} = 5\pi$ *rad*). As a result, the electromagnetic torque produced by this winding set excess the load torque. Consequently, the *XYZ* winding set must compensate for this additional torque and operates in the generating operation mode. From (9), I_{qs1} could be calculated as:

$$I_{qs1} = \frac{-L_{m1}}{L_{s1}} I'_{qr1} \quad (38)$$

Consistent with (15) and assuming $\frac{d\lambda'_{qr1}}{dt} = 0$ in the steady-state condition, I'_{qr1}can be calculated as:

$$I'_{qr1} = \frac{-\omega_{sl}\lambda'_{dr1}}{R'_{r1}} \quad (39)$$

Where $\omega_{sl} = \omega_{r\min} - \omega_r^*$. Substituting (39) into (38) and neglecting the leakage flux, I_{qs1} is approximately:

$$I_{qs1} \approx \frac{L_{m1}}{L_{s1}} \frac{\omega_{sl}\lambda_{ds1}}{R'_{r1}} \quad (40)$$

According to (40) and (20), the reference electromagnetic torque for the ABC winding set and the reference q-axis voltage for this winding set are calculated as (41) and (42), respectively.

$$T_{e1}^* = k_1 \frac{L_{m1}}{L_{s1}} \frac{\omega_{sl}\lambda_{s1}^*}{R'_{r1}} \lambda_{s1}^* \quad (41)$$

$$V_{qs1}^* = R_{s1} \frac{L_{m1}}{L_{s1}} \frac{\omega_{sl}\lambda_{s1}^*}{R'_{r1}} + \omega_{r\min}\lambda_{s1}^* \quad (42)$$

According to the above discussions and considering $\frac{d\omega_r^*}{dt} = 0$ in this mode of operation, the reference electromagnetic torque for the *XYZ* winding set is determined as:

$$T_{e2}^* = -T_{e1}^* + T_{load} + B\omega_r^* \quad (43)$$

The q-axis reference voltage for *XYZ* winding set equals:

$$V_{qs2}^* = R_{s2} \frac{T_{e2}^*}{k_2\lambda_{s2}^*} + \omega_{s2}\lambda_{s2}^* \quad (44)$$

The proposed torque-sharing algorithm is straightforward and has just one decision factor (the reference speed) and two calculation steps. Thus, it is easy to implement. The only difficulty in the experimental implementation is that it requires the load torque information. However, its exact value is not necessary and the ΔC matrix will compensate for the possible disturbances in the load torque value.

IV. Sliding Mode Full Order Observer

One of the most important concerns in drive systems is speed and position sensors elimination. Generally, sensor-less control schemes result in high reliable, better noise immune and cost-effective drive systems. DSWIM sensor-less control has been addressed in some references [13] and [20]–[22]. In [20] the position and speed sensor elimination has been realized through the Direct Calculation Method (DCM). This method is based on rotor flux estimation. The simplicity and small computational time are the main advantages of this method. However, it is very sensitive to machine parameters especially the stator resistance. Moreover, it requires ideal integral and actual stator voltages, the

measurement of which due to the PWM and the influence of dead time is very difficult. Accordingly, its accuracy is low, especially in very low speed region. The Model Reference Adaptive System (MRAS) is adapted for speed estimation of DSWIMs in [13], [21] and [22]. The MRAS based speed estimation methods are easy to implement and their adaptation speed is high. Even though, their implementation requires the exact machine parameters and they are sensitive to machine parameters variation. Accordingly, the machine parameters variation highly influences their accuracy.

One of the most promising types of sensor-less observers in IM control systems are Sliding Mode Observers (SMOs) which have significant superiorities over other Observers, such as robust performance against un-modeled dynamics and parameters variations, disturbance rejection and fast dynamic response [17]. SMOs are variable structure control systems and commonly they estimate some state variables (flux and current) based on the measured terminal parameters (voltages and currents).

In general, a SMO can be implemented in various reference frames. Typically, SMOs adapt IM models in a single frame and they estimate the stator flux, in the first step. After that, the rotor flux and the stator current are estimated and finally the rotor speed is calculated. Consequently, the estimated speed may involve uncertainties due to the aggregated errors, noise and delays. Since this imprecise speed is fed backed to the pervious observation steps, the total accuracy of the observer is deteriorated. In [18] it is declared that the application of two reference frames for stator flux and rotor speed independent estimation, can resolve this difficulty. In this paper, a full order SMO is implemented that adapts two reference frames: stationary reference frame and the rotor flux reference frame. This observer is able to estimate the rotor speed, stator winding fluxes and stator fluxes orientation angles.

A. Stator Fluxes Estimation

The stator flux of the i[th] winding set is estimated in the stationary reference frame as:

$$\frac{d\hat{\lambda}_{si}}{dt} = -R_{si}\hat{i}_{si} + U_i + (\gamma_{i1} + j\gamma'_{i1}\omega_r^*)\, sign(i_{si} - \hat{i}_{si}) \tag{45}$$

In (45) the stator winding currents are estimated as:

$$\hat{i}_{si} = \frac{L'_{ri}\hat{\lambda}_{si} - L_{mi}\hat{\lambda}_{ri}}{L_{\delta i}^2} \tag{46}$$

Where, $\hat{\lambda}_{ri}$ stands for the estimated rotor flux in the stationary reference frame and it is calculated as:

$$\hat{\lambda}_{ri} = \frac{L_{ri}\hat{\lambda}_{si} - L_{\delta i}^2 i_{si}}{L_{mi}} \tag{47}$$

Consequently, following equations (45) to (47), the stator winding fluxes can be conveniently estimated independent of the rotor speed.

B. Flux Angle Determination

The block-diagram of the proposed flux angle determination technique is shown in Fig. 5. Consistent with the torque-sharing

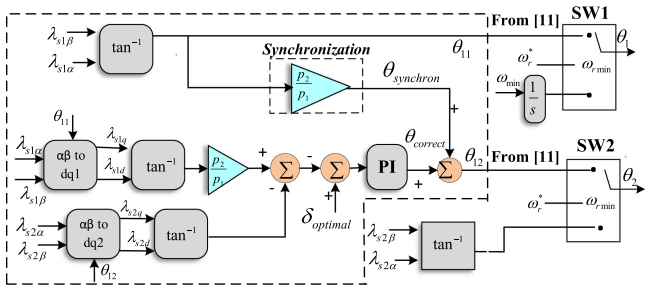

Fig. 5. The proposed flux angle determination technique.

algorithm, two operation modes are also considered for this part of the DSWIM drive system: synchronous and asynchronous.

a) Synchronous mode: in this mode of operation, switches SW1 and SW2 connect their output to their upper side of their input. As previously stated, the optimal iron utilization in a DSWIM occurs if the winding fluxes be synchronized and their relative position (δ) be 180^o [6]. In [11] this condition is guaranteed through optimal reference frame angle determination. In this paper, a similar process is implemented for flux angle determination in the synchronous mode. As it is illustrated, in this method the flux angle of the *ABC* is determined first. This angle is multiplied by the pole pair ratio of the winding sets to guarantee the flux synchronization. In the next step, the optimal relative position is assured through a Proportional Integral (PI) controller. The output of this controller is shown by $\theta_{correct}$ in Fig. 5. The *ABC* winding flux orientation angle is determined as:

$$\hat{\theta}_1 = \tan^{-1}\left(\frac{\hat{\lambda}_{s\beta 1}}{\hat{\lambda}_{s\alpha 1}}\right) \tag{48}$$

As a result, the *XYZ* winding flux orientation angle is calculated as (49).

$$\hat{\theta}_2 = \frac{p_2}{p_1}\hat{\theta}_1 + \theta_{correct} \tag{49}$$

b) Asynchronous mode: in the asynchronous mode SW1 and SW2, connect their output to their lower input and the frequency of the ABC winding set is fixed to ω_{min}. Thus, $\hat{\theta}_1$equals:

$$\hat{\theta}_1 = \int \omega_{\min} dt \tag{50}$$

In this mode of operation, the synchronization of winding fluxes is lost. Accordingly, $\hat{\theta}_2$ is independently calculated as:

$$\hat{\theta}_2 = \tan^{-1}\left(\frac{\hat{\lambda}_{s\beta 2}}{\hat{\lambda}_{s\alpha 2}}\right) \tag{51}$$

C. Rotor Speed Estimation

Since the winding sets of a DSWIM share a common rotor, the rotor speed can be estimated according to each them. In this paper, the rotor speed estimation is done according to the *ABC* winding set. The rotor speed can be calculated as the difference between the synchronous speed and the slip speed.

$$\hat{\omega}_r = \hat{\omega}_s - \hat{\omega}_{slip} \tag{52}$$

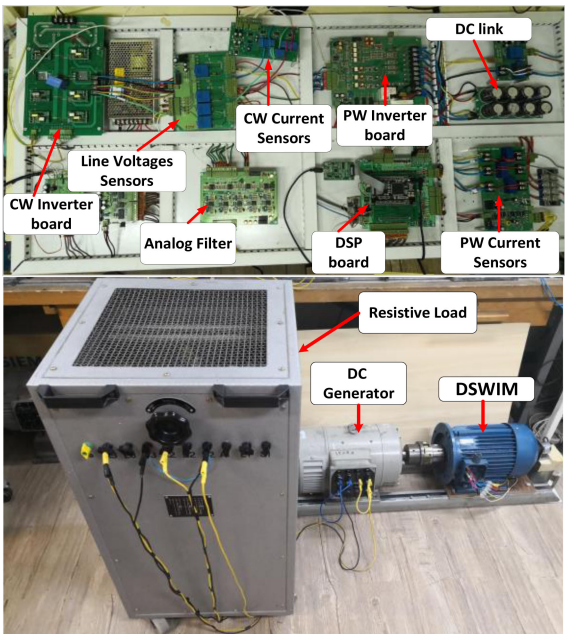

Fig. 6. Experimental test bench.

Where, $\hat{\omega}_{slip}$ is the slip speed and it is determined as (53).

$$\hat{\omega}_{slip} = \frac{2R_{r1}\hat{T}_{e1}}{3P\hat{\lambda}_{r1}^2} \tag{53}$$

In (53), $\hat{T}_{e1}$stands for the estimated electromagnetic torque produced by the *ABC* winding set and it equals:

$$\hat{T}_{e1} = \frac{3P_1}{2}\left(\hat{\lambda}_{sd1}i_{sq1} - \hat{\lambda}_{sq1}i_{sd1}\right) \tag{54}$$

The synchronous speed is estimated adapting a discrete form as follows:

$$\hat{\omega}_s = \frac{\hat{\lambda}_{rd1}(k-1)\hat{\lambda}_{rq1}(k) - \hat{\lambda}_{rq1}(k-1)\hat{\lambda}_{rd1}(k)}{T_s\hat{\lambda}_{r1}^2} \tag{55}$$

In (55) *k* and *k-1* stand for the present and the previous samples, respectively and T_s represents the sampling period duration.

V. Results

The performance of the proposed DSWIM drive system is evaluated through some experimental tests. Fig. 6 illustrates the experimental test bench. In this figure, Power Winding (PW) and Control Winding (CW) stand for the *ABC* and *XYZ* winding sets, respectively. The DSWIM under study is a 3.3kW laboratory prototype. Table I shows the nominal parameters of this machine and its detailed specifications are given in [19]. In this system, a DC generator supplying a resistive load is adapted as a load for the DSWIM. The modular drive system includes two voltage source inverters supplying the PW and the CW. In addition, the phase currents of the winding sets are measured through their corresponding current sensor boards, each of which include three LEM LTS-6- NP current sensors. A common voltage sensor board is adapted for the two winding sets. This board

TABLE I
DSWIM Nominal Values and Parameters [19]

Parameter	Value	
	ABC	XYZ
Number of poles	2	6
Output Power (W)	2830	500
Voltage Frequency (Hz)	50	150
RMS Line Voltage (V)	300	50
Phase Current (A)	9	5
Rotor Speed (rpm)	2830	
Efficiency	88%	
Nominal Torque (N.m)	11.15	
Moment of inertia (kg.m^2)	0.02	

is comprised of four LEM LV-25-P sensors. Indeed, the voltage measurement is based on the symmetrical operation. Two line voltages of each winding set is measured and the third one is calculated based on the two others. As illustrated in Fig. 6, this drive system is also provided with a low-pass second order analog filter, through which the output signals of the current sensors and the voltage sensors are passed. The key module of this drive system is the Digital Signal Processor (DSP) board that is of the type TMS320F28335. This board is the interface among various modules of the drive system and sends the appropriate switching commands to the inverter boards according to the measured signals and the programmed control scheme.

Fig. 7 illustrates the experimental results. Fig. 7(a) depicts the *ABC* winding estimated flux when its reference varies step-wisely at $t = 2s$, while the estimated flux of the *XYZ* winding set is shown in Fig. 7(b) for a reference step change at $t = 3s$. As it is clear from Figs. 7(a) and (b), the proposed STSMC can properly control the winding fluxes. Moreover, the chattering is very low and the flux controllers have high-speed dynamic responses.

The estimated and the reference speeds are shown in Fig. 7(c). As illustrated, in the first second, the rotor speed is kept at zero and DSWIM operates in the asynchronous operation mode. Afterward, it increases with a ramp pattern up to 200 rad/s. Then, it decreases with a same pattern and accelerates in the reverse direction up to 200 rad/s and it is kept at this speed until $t = 10s$. Fig. 7(c) verifies that the proposed control scheme can appropriately control the rotor speed in different operation modes and in a wide speed range, including zero speed.

Figs 7(d) and (e) stand for the calculated electromagnetic torques produced by the *ABC* and the *XYZ* winding sets, respectively. As stated previously, the DSWIM load is a separately exited DC generator supplying a resistive load. Generally, the DC machine generated voltage is proportional to its rotor speed. Thus, neglecting the DC generator losses, the load torque and the armature voltage are obtained as (56) and (57), respectively.

$$T_R = \frac{P_R}{\omega_r} = \frac{V_{ar}^2}{R_{Load}\omega_r} \tag{56}$$

$$V_{ar} = k_{ar}\phi_{DC}\omega_e \tag{57}$$

In (57) k_{ar} is a constant value. If the voltage of the excitation winding of the DC generator is kept constant, the DC generator flux (ϕ_{DC}) can also considered constant. If the DC generator

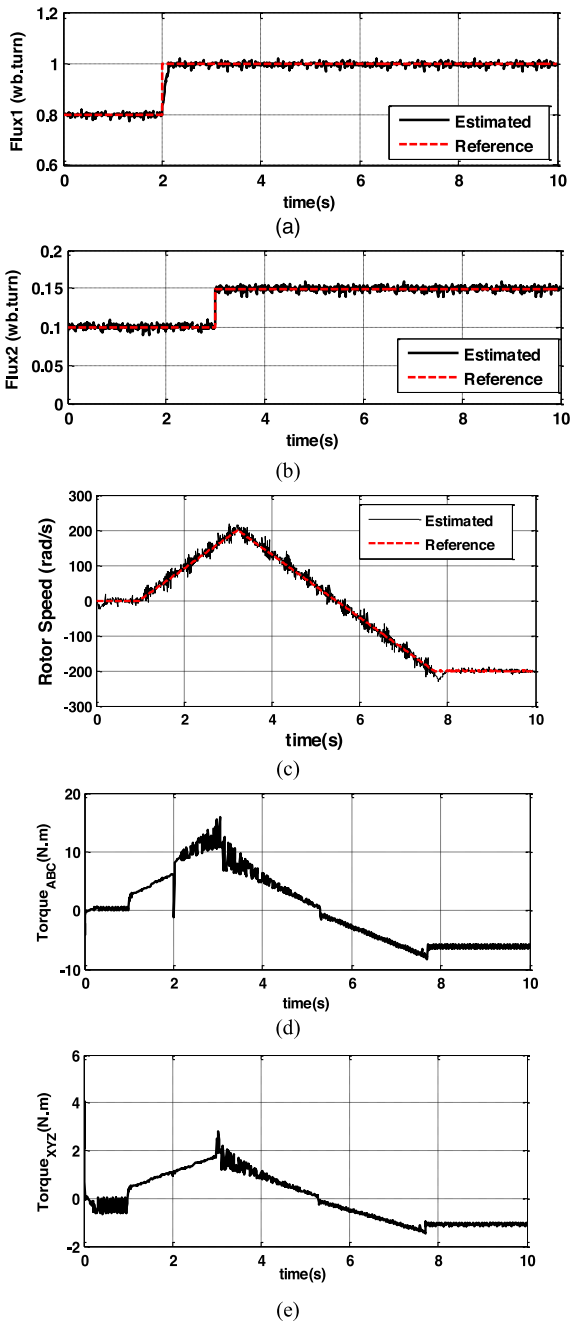

Fig. 7. Experimental results a) PW flux b) CW flux c) rotor speed d) PW electromagnetic torque e) CW electromagnetic torque.

has p poles, $V_{ar} = k_{ar}\phi_{DC}\frac{p}{2}\omega_r$. Thus:

$$T_R = \frac{\left(k_{ar}\phi_{DC}\frac{p}{2}\right)^2}{R_{Load}}\omega_r = k^*\omega_r \tag{58}$$

Where, $k^* = \frac{(k_{ar}\phi_{DC}p)^2}{4R_{Load}}$. For the proposed system with $R_{Load} = 18\Omega$, k^*equals 0.0335. Eq. (58) shows that in the experimental tests, the load torque has an approximately linear relation with the rotor speed. This is also shown in Figs. 7(d) and (e). According to (58), in the asynchronous operation region (before $t = 1s$), the load torque is approximately zero and the DSWIM electromagnetic torque overcomes the zero speed losses torque. As it is clear from Fig. 7, clamping the frequency of ABC winding set at 5 rad/s results in larger electromagnetic torque produced by this winding than the required load torque. In this condition, the torque-sharing algorithm fixes the XYZ winding electromagnetic torque at a negative value to ensure the torque balance and accordingly accurate speed control in this mode of operation. In the synchronous operation mode, the electromagnetic torque waveforms of the two winding sets are similar to each other and their ratio is 5.7. As their synchronous speed is equal, their power ratio is also 5.7. As a result, both winding sets cooperate to supply the required power by a ratio equal to their power ratings. In the steady-state condition ($8<t<10$), $T_{Load} = 6.7N.m$. From Figs. 7(d) and (e), the electromagnetic torques produced by the *ABC* and *XYZ* winding sets are 6.12N.m and 1.08, respectively. Although the produced torques have the desired ratio, the DSWIM electromagnetic torque (sum of ABC and XYZ electromagnetic torques) is more than the load torque by *0.5 N.m*. Indeed, this extra torque overcomes the torque that is the result of the DC machine and DSWIM losses.

The proposed controller is designed based on the nominal machine parameters. However, some machine parameters vary as the temperature changes or the core of machine inters the saturation region. In addition, the load torque may have sudden changes. The variable machine parameters, the alteration of which may influence the proposed controller performance are *J*, R_{si} and *B*. As *J* and *B* appear in the first row of F and D, their variations may influence the rotor speed control. To evaluate the robustness of the proposed control system, these parameters are changed by 50% from their nominal value. As the controlled variations of *J* and *B* is not achievable in the experimental tests, the effect of their variations is evaluated in a simulated system in MATLAB/SIMULINK. It worth noting that, in the simulated system, the parameters of the controller remained unchanged, while *J* and *B* in the simulated DSWIM are changed by 50% from their rated values. Fig. 8(a) shows the rotor speed and its reference command in this condition. As it is illustrated, in this test the rotor speed is kept at zero, first. After that, it ramps up to the nominal speed. Then, it ramps dawn and accelerates in the reverse direction. Again, it ramps up to zero speed and kept at this value until the end of simulation. As it is clear from this figure, the proposed control system can appropriately control the rotor speed, despite the variations applied to the parameters J and B.

The robustness of the control method against the R_{s1} and R_{s2} uncertainties appear in the second and third row of the D and F, respectively As a result, their variation may influence the winding fluxes control. To assess the robustness of the proposed controller against the variations of these parameters, some simulations executed. In this case, R_{s1} and R_{s2} have changed by 30% from their nominal values in the simulated DSWIM, while the controller parameters remained unchanged. Figs 8(b) and (c) illustrate the ABC and XYZ windings fluxes and their reference commands, respectively. Fig 8(b) shows the ABC winding flux for two-step changes. The first step change is positive and occurs at $t = 2s$ and the following is negative and occurs at $t = 5s$. However, similar to the experimental tests, a single step change

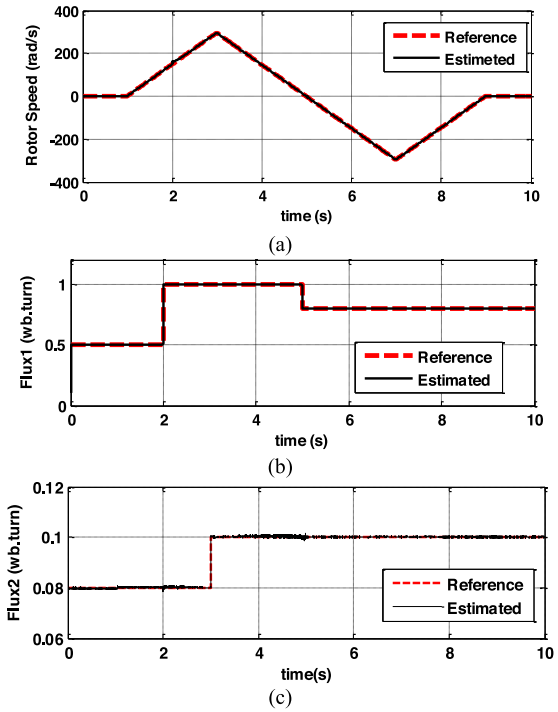

Fig. 8. simulation results in J, B and R_{si} variation condition a) rotor speed b) PW flux c) CW flux.

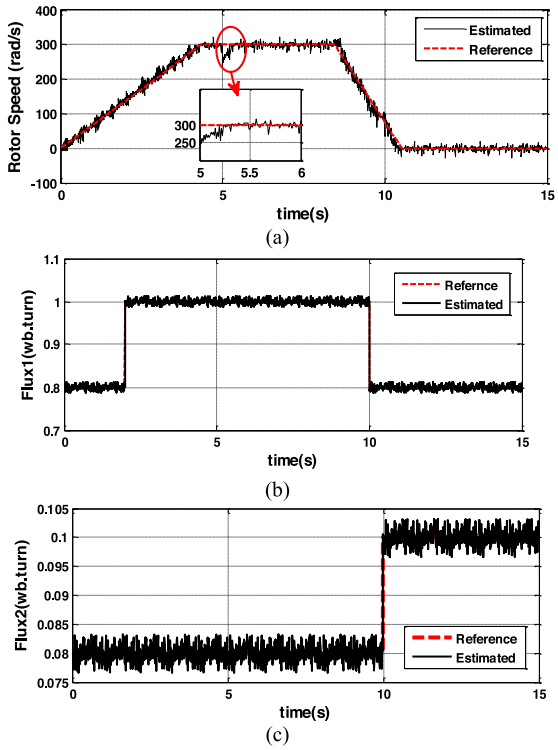

Fig. 9. experimental results in step load change condition a) rotor speed b) PW flux c) CW flux.

TABLE II
COMPARISON OF VARIOUS DSWIM DRIVE SYSTEMS

Reference	Control strategy	Sensor dependency	Robustness	Optimal flux condition
[5] & [7]	scalar	Position	low	No
[6] &[8-10]	IFOC	Position	low	Yes
[11]	FOC	Position	low	Yes
[12]	IOFL	Speed	low	No
[13], [21] & [22]	IOFL	Sensor-less	low	No
[14]	PI-SMC	Speed	high	No
The proposed research work	STSMC	Sensor-less	high	Yes

is considered for the XYZ winding set at $t = 3s$ (Fig. 8(c)). Consistent with Fig. 8, the proposed controller is also robust against stator resistance variations.

The robustness of the proposed control system against load torque variation is evaluated through an experimental test, in which a step change occurred for the load torque. This has been achieved through applying a sudden change to the terminal resistance supplied by the DC machine. Fig. 9 illustrates the rotor speed and winding fluxes for a step change in the load torque at $t = 5s$. As it is clear from Fig. 9(a), at $t = 5s$ the rotor speed experiences a 50 rad/s drop for about 0.2s and after that it properly follows its reference command. Figs 9(b) and (c) confirm that the winding fluxes do not sense the step change occurred in the load torque and they appropriately follow their reference commands. Table II compares the proposed DSWIM drive system with other DSWIM drive systems proposed in literature from different aspects.

VI. CONCLUSION

A novel non-liner DSWIM drive system was proposed. The proposed drive system was able to truthfully control the rotor speed and winding fluxes through a STSMC. In addition, this system was provided with a full order SMO. The proposed observer could precisely estimate the rotor speed and winding fluxes in various speed regions. Besides, it guaranteed for the optimal flux condition. Moreover, a novel torque-sharing algorithm for DSWIMs was introduced, which enabled them to operate in a wide speed region, including zero speed operation region, without any overloading in winding sets. The proposed drive system was implemented on a 3.3kW laboratory prototype DSWIM. The experimental results confirm the functionality of the proposed drive system in various operation regions. Implementing STSMC guaranteed the control system Lyapunov stability. Accordingly, in the case of mechanical and electrical machine parameters variation, the proposed control scheme could properly control the rotor speed and winding fluxes at their reference commands.

REFERENCES

[1] S. Basak, and C. Chakraborty, "Dual stator winding induction machine: Problems, progress, and future scope," *IEEE Trans. Ind. Electron.*, vol. 62, no. 7, pp. 4641–4652, Jul. 2015.

[2] H. Mosaddegh Hesar, H. Abootorabi Zarchi, and G. A. Markadeh, "Modeling and dynamic performance analysis of brushless doubly fed induction machine considering iron loss," *IEEE Trans. Energy Convers.*, vol. 35, no. 1, pp. 193–202, Mar. 2020.

[3] M. Yousefian, H. A. Zarchi, and H. Gorginpour, "Modified steady-state modelling of brushless doubly-fed induction generator taking core loss components into account," *IET Electric Power Appl.*, vol. 13, no. 9, pp. 1402–1412, Sep. 2019.
[4] M. Moradian and J. Soltani, "An isolated three-phase induction generator system with dual stator winding sets under unbalanced load condition," *IEEE Trans. Energy Convers.*, vol. 31, no. 2, pp. 531–539, Jun. 2016.
[5] A. Munoz-Garcia and T. A. Lipo, "Dual stator winding induction machine drive,"in *Proc. Conf. Rec. 1998 IEEE Ind. Appl. Conf., 33rd IAS Annu. Meeting (Cat. No.98CH36242)*, vol. 1, St. Louis, MO, USA, 1998, pp. 601–608.
[6] J. M. Guerrero and O. Ojo, "Total airgap flux minimization in dual stator winding induction machines," *IEEE Trans. Power Electron.*, vol. 24, no. 3, pp. 787–795, Mar. 2009.
[7] A. R. Munoz and T. A. Lipo, "Dual stator winding induction machine drive," *IEEE Trans. Ind. Appl.*, vol. 36, no. 5, pp. 1369–1379, Sep./Oct. 2000.
[8] J. M. Guerrero and O. Ojo, "Flux level selection in vector-controlled dual stator winding induction machines," *IET Electric Power Appl.*, vol. 3, no. 6, pp. 562–572, Nov. 2009.
[9] J. M. Guerrero and O. Ojo, "Air-gap flux density optimization in dual stator winding induction machines," in *Proc. IEEE Power Electron. Specialists Conf.*, Rhodes, 2008, pp. 3767–3773.
[10] J. M. Guerrero and O. Ojo, "Total Air-gap flux minimization in dual stator winding induction machines," in *Proc. 23rd Annu. IEEE Appl. Power Electron. Conf. Expo.*, Austin, TX, 2008, pp. 1132–1138.
[11] M. Ayaz Khoshhava, H. Abootorabi Zarchi, and G. R. Arab Markadeh, "Optimal reference frame angle approach for air-gap flux minimization in dual stator winding induction machines," *IEEE Trans. Power Electron.*, vol. 35, no. 7, pp. 6658–6662, Jul. 2020.
[12] O. Ojo and Z. Wu, "Speed control of a dual stator winding induction machine," *APEC 07 - 22nd Annu. IEEE Appl. Power Electron. Conf. Expo.*, Anaheim, CA, USA, 2007, pp. 229–235.
[13] Z. Wu, O. Ojo, and G. Dong, "MRAS speed estimation and full-order flux observer for dual stator winding induction motor drives," in *Proc. IEEE Power Electron. Specialists Conf.*, Orlando, FL, 2007, pp. 2428–2434.
[14] M. Ayaz and H. Abootorabi, "Direct torque control of dual stator winding induction machine based on PI-Sliding mode control," in *Proc. Elect. Eng. (ICEE), Iranian Conf.*, Mashhad, 2018, pp. 1233–1239.
[15] C. Lascu, I. Boldea, and F. Blaabjerg, "Variable-structure direct torque control - A class of fast and robust controllers for induction machine drives," *IEEE Trans. Ind. Electron.*, vol. 51, no. 4, pp. 785–792, Aug. 2004, doi: 10.1109/TIE.2004.831724.
[16] M. Ayaz Khoshhava, H. Abootorabi, and G. A. Markadeh, "Optimal design of a dual stator winding induction motor with minimum rate reduction level," *IEEE Trans. Ind. Electron.*, vol. 68, no. 2, pp. 1016–1024, Feb. 2021.
[17] M. Zaky and M. M. Khater, "Review of different speed estimation schemes for sensorless induction motor drives," *J. Elect. Eng.*, vol. 3, no. 1, pp. 1–39, 2008.
[18] C. Lascu, I. Boldea, and F. Blaabjerg, "Direct torque control of sensorless induction motor drives: A sliding-mode approach," *IEEE Trans. Ind. Appl.*, vol. 40, no. 2, pp. 582–590, Mar./Apr. 2004.
[19] M. Ayaz Khoshhava, H. Abootorabi, and G. R. Arab Markadeh, "Iron loss modeling in dual stator winding induction machines with unequal pole pairs and squirrel cage rotor," *IEEE Trans. Ind. Electron.*, vol. 68, no. 4, pp. 2931–2941, Apr. 2021.
[20] S. Chatterjee and S. Chatterjee, "A novel speed sensor-less vector control of dual stator induction machine with space vector based advanced 9-zone hybrid PWM for grid connected wind energy generation system," *Electric Power Syst. Res.*, vol. 163, pp. 174–195, 2018.
[21] M. Vazifehdan, H. A. Zarchi, and M. A. Khoshhava, "Sensorless vector control of induction machines via sliding mode control based model reference adaptive system," in *Proc. 28th Iranian Conf. Elect. Eng. (ICEE)*, Tabriz, Iran, 2020, pp. 1–6.
[22] M. Vazifedan, H. A. Zarchi, and M. A. Khoshhava, "Sensorless control of dual stator winding induction machine drive using sliding mode control based model reference adaptive system," in *Proc. 11th Power Electron., Drive Syst., Technol. Conf. (PEDSTC)*, Tehran, Iran, 2020, pp. 1–7.
[23] Z. Wu, O. Ojo, and J. Sastry, "High-Performance control of a dual stator winding DC power induction generator," *IEEE Trans. Ind. Appl.*, vol. 43, no. 2, pp. 582–592, Mar./Apr. 2007.
[24] Z. Wu and O. Ojo, "High performance control of a dual winding induction generator with series connected boost rectifiers," in *Proc. 37th IEEE Power Electron. Specialists Conf.*, Jeju, 2006, pp. 1–7.
[25] A. Benchaib, A. Rachid, E. Audrezet, and M. Tadjine, "Real-time sliding-mode observer and control of an induction motor," *IEEE Trans. Ind. Electron.*, vol. 46, no. 1, pp. 128–137, Feb. 1999.
[26] R. Sadeghi, S. M. Madani, M. Ataei, M. R. Agha Kashkooli, and S. Ademi, "Super-Twisting sliding mode direct power control of a brushless doubly fed induction generator," *IEEE Trans. Ind. Electron.*, vol. 65, no. 11, pp. 9147–9156, Nov. 2018.
[27] A. Chalanga, S. Kamal, L. M. Fridman, B. Bandyopadhyay, and J. A. Moreno, "Implementation of super-twisting control: Super-twisting and higher order sliding-mode observer-based approaches," *IEEE Trans. Ind. Electron.*, vol. 63, no. 6, pp. 3677–3685, Jun. 2016.

Mojtaba Ayaz Khoshhava received the B.Sc. degree in electrical engineering from the Ferdowsi University of Mashhad, Mashhad, Iran, in 2014, the M.Sc. degree in electrical engineering from Shiraz University, Shiraz, Iran, in 2014, and the Ph.D. degree in electrical engineering from the Ferdowsi University of Mashhad, in 2020. His research interests include electrical machine design, power electronics, and variable-speed drives.

Hossein Abootorabi Zarchi received the Ph.D. degree from the Isfahan University of Technology, Isfahan, Iran. From May 2009 to February 2010, he was a Visiting Ph.D. Student with the Control and Automation Group, Denmark Technical University, Denmark. He is currently an Assistant Professor with the Faculty of Engineering, Ferdowsi University of Mashhad, Mashhad, Iran. His research interests include renewable energies, electrical machines, and applied nonlinear control in electrical drives.

Gholamreza Arab Markadeh received the B.Sc., M.Sc., and Ph.D. degrees in electrical engineering from the Isfahan University of Technology, Isfahan, Iran, in 1996, 1998, and 2005, respectively. He is currently an Associate Professor with the Faculty of Engineering, Shahrekord University, Shahrekord, Iran. His research interests include nonlinear control, power electronics, and variable-speed drives. He is the Editor-in-Chief of the *Journal of Dam and Hydroelectric Powerplant*. He was the recipient of the IEEE Industrial Electronics Society IECON'04 Best Paper Presentation Award in 2004.